

Confocal microscopy of geometrically frustrated hard sphere crystals

Roel P.A. Dullens^{1,2}, Volkert W.A. de Villeneuve¹, Maurice C.D. Mourad¹, A.V. Petukhov¹ and Willem K. Kegel¹

¹ Van 't Hoff Laboratory for Physical and Colloid Chemistry, Debye Institute, Utrecht University, Padualaan 8, 3584 CH Utrecht, The Netherlands

² 2. Physikalisches Institut, Universität Stuttgart, 70569 Stuttgart, Germany

Received: date / Revised version: date

Abstract. Confocal microscopy has been used to study the crystallization of two colloidal model systems that are geometrically frustrated in a completely different way: (I) hard colloidal polyhedrals, where crystallization is frustrated due to the incommensurate particle shape and (II) large spherical impurities in a sea of monodisperse colloidal hard spheres, where crystallization is frustrated by the introduction of impurities. As a reference system, we analyzed the crystallization of pure monodisperse colloidal hard spheres. We show that although the crystal structures of both systems are highly dissimilar on the individual particle level, both sources of geometrical frustration have a similar effect on the structure on the grain level. We quantitatively characterize the polycrystalline structures and study the crystallization process in time. Whereas grain boundaries persist in the frustrated systems due to structural arrest, the majority of grain boundaries anneals out quite rapidly in the reference system. Therefore, we argue that both sources of geometrical frustration cause a polycrystalline structure.

PACS. 61.72 Mn Grain and twin boundaries – 61.82 Rx Nanocrystalline materials – 82.70 Dd Colloids

1 Introduction

Crystals are characterized by perfect periodic order. However, in practice crystals always exhibit various types of imperfections or defects such as vacancies, dislocations, stacking faults, grain boundaries and impurities [1]. Defects can arise since these are frozen in during crystal growth or formed due to stress on the crystal. Furthermore, they strongly influence macroscopic properties of many materials like semiconductors, metals and ceramics [2]. Grain boundaries in crystals crucially influence the mechanical properties, as the grain size is directly related to the strength of materials [1–4]. For relatively small grain sizes the strength increases with increasing grain size [4–6], while for larger grain sizes the materials strengthens if the crystallites gets smaller (Hall-Petch effect) [7, 8]. Therefore, controlling the grain size, for instance by tuning the solidification rate, heating or mechanical annealing, is of paramount importance in material science [1, 3, 9, 10].

Studying grain boundary formation and grain growth in atomic and molecular crystals in real-space is rather difficult due to the small length scales involved in atomic and molecular systems. Consequently, computer simulations have proven to be beneficial to study these issues on the atomic level [11–17]. Inherent to their typical size, colloidal systems provide an excellent tool to address these issues experimentally. In contrast to atomic systems, col-

loidal systems consist of particles with a characteristic size between a nanometer and several micrometers. This length scale makes them very suitable to be studied in real-space and real-time by microscopy techniques [18–20]. In particular, the combination of advanced colloidal particles and confocal microscopy has already made it possible to study several fundamental condensed matter problems, such as freezing, melting and glass formation, on the single-particle level [10, 18–32]. Interestingly, colloidal systems exhibit similar phase-behaviour as atomic systems, making colloids a powerful model-system for condensed matter and atomic materials [33–36].

In this work, we consider two colloidal model systems that exhibit completely different types of geometrical frustration: the crystals of the colloidal polyhedrals are frustrated due to incommensurate particle shape [37], whereas the crystals in the second system are frustrated by the addition of model impurities [28, 30]. The influence of particle shape is e.g. relevant for applications in powder technology and ceramics [38], while the colloidal crystal containing impurities may serve as a model system for nanocrystalline materials containing dopants [15–17, 39]. In our previous work we studied the structure of single crystalline domains of hard polyhedral colloids, without considering grain boundaries [37]. Furthermore, we addressed the influence of the presence of impurities on the dynamics of crystallization of colloidal hard spheres, without quantita-

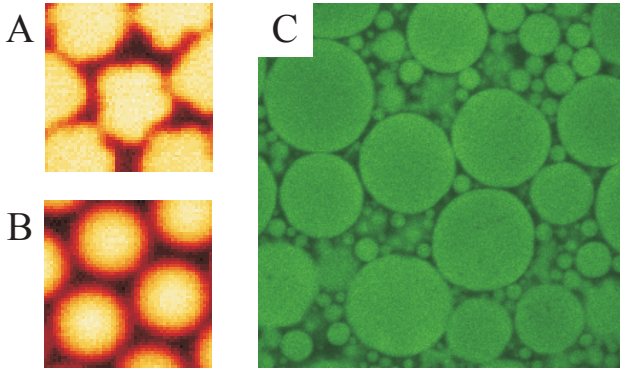


Fig. 1. Confocal microscopy images of (A) the polyhedral particles and (B) the spherical reference particles ($9 \times 9 \mu\text{m}^2$). (C) Confocal image of the impurities ($70 \times 70 \mu\text{m}^2$) directly after synthesis. The larger particles (i.e. $d_i \in 7.5 - 31.5 \mu\text{m}$) were used as model impurities in a sea of small monodisperse particles ($d_p = 1.5 \mu\text{m}$).

tively analyzing the final crystal structure [28,30]. Here, we use real-space confocal microscopy [40] to quantitatively characterize the polycrystalline structure of geometrically frustrated colloidal crystals. Our results clearly show that both sources of geometrical frustration—which are completely different in nature—significantly reduce the grain size of the colloidal crystals in a very similar way. In addition, we investigate the arrested grain growth by identifying the (time-dependent) defect-structure during grain growth.

2 Experimental

The ‘*polyhedral system*’ consists of crosslinked and fluorescently labeled polymethyl methacrylate (PMMA) colloids that are monodisperse in size, but exhibit a polyhedral particle shape [37,41] (see Fig. 1 A). In our experiments, we compare the polyhedrals to a reference system of spherical and size-monodisperse reference PMMA particles of equal size [42] (see Fig. 1B). The diameters d of the polyhedral and reference particles are respectively $d = 2.23 \pm 0.09$ and $d = 2.33 \pm 0.07$. The ‘*impurity system*’ consists of a sea of fluorescently labeled monodisperse PMMA particles with a diameter d_p of $1.5 \pm 0.09 \mu\text{m}$ containing a small fraction of very large PMMA particles, called the impurities [28,30]. The impurities were obtained by a synthesis following [42]. The resulting particles were extremely polydisperse and very large ($d_i \in 0.1 - 100 \mu\text{m}$) as illustrated in Fig. 1C. Impurities of different sizes were separated by repeated sedimentation. Subsequently a small amount (typically < 0.1 weight %) of impurities of the desired size was added to a sea of small PMMA particles. As a result, systems of monodisperse PMMA spheres contaminated with differently sized model impurities were obtained. Obviously, the reference system is formed by the same monodisperse PMMA spheres ($d_p = 1.5 \mu\text{m}$) without impurities. The impurity systems are characterized by the size ratio between the particles and the impurities

$\alpha \equiv (d_i/d_p)m$ with d_i and d_p respectively the diameters of the impurity and the particles. In this work, we consider impurity systems with $\alpha = 5, 8, 13$ and 21 .

The colloidal model systems were dispersed in a mixture of cis-decalin (Merck, for synthesis), tetralin (Merck, for synthesis) and carbontetrachloride (Merck, for spectroscopy), which simultaneously matches the refractive index and almost the mass density of the particles [30,43]. In this solvent the particles interact via a hard-sphere-like potential [43,44]. The dispersions were contained in small homemade vials [43] and the particles were imaged using a Nikon TE 2000U inverted microscope with a Nikon C1 confocal scanning laser head. For the polyhedral colloids, samples with a volume fraction $\phi \equiv \rho v \approx 0.40$ were prepared (with ρ the number density and v the particle’s volume). The impurity systems were prepared at relatively high volume fraction ($\phi \approx 0.55$) to minimize the mobility of the impurity during the measurements [28,30]. The volume fractions of the samples were defined relative to the random close packing density at the relevant polydispersity [45].

In the polyhedral, the impurity and the reference systems the colloidal crystal heterogeneously nucleates at the wall, followed by subsequent upward growth [28,30,32,46]. As a result, the (111)-plane of the crystal is oriented at the wall, allowing a quantitative 2D in-plane analysis of the systems [24,28,30,37,46,47]. The structure of the polyhedrals was analyzed after slow sedimentation had fully completed as the influence of the particle shape is most pronounced at highest compression. Since the layering in the polyhedral system did not persist in bulk [37], we studied the first layer at the glass wall in this system. Although certainly interesting, the question as to how the structure of the polyhedrals evolves in the third dimension lies outside the scope of this work. The impurity system was studied in the plane corresponding to the center of the impurity, which was typically $20 \mu\text{m}$ above the glass wall. Furthermore, we studied the time-dependent structure of both systems during crystallization. The centers of the particles were located using image-analysis software similar to that described in [48]. We verified that the polyhedral particle shape did not significantly affect the accuracy of the particle tracking.

3 Results and discussion

Representative confocal micrographs of the colloidal crystal formed by the frustrated and reference systems are shown in Fig. 2. The structure of both the polyhedrals and the impurity system exhibit a much higher degree of polycrystallinity compared to the structure formed by the reference spheres. To quantify this, we computed the radial distribution function $g(r)$ (being proportional to the probability of observing a particle a distance r away from a given particle):

$$g(r) = \frac{1}{\rho} \left\langle \sum_{j \neq i} \delta(r_i - r_j - r) \right\rangle. \quad (1)$$

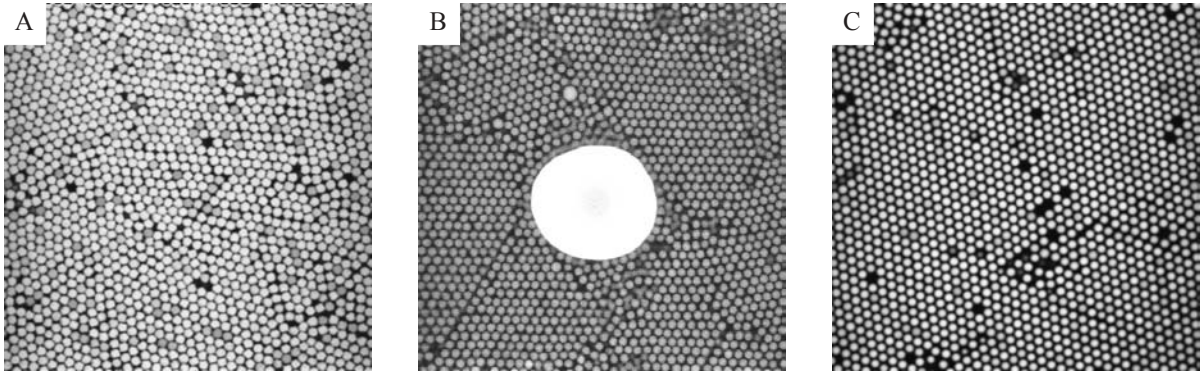


Fig. 2. Representative confocal images of (A) the polyhedrals ($75 \times 75 \mu\text{m}^2$) and (B) the impurity system for $\alpha = 13$ ($60 \times 60 \mu\text{m}^2$) and (C) the reference spheres for the polyhedrals ($75 \times 75 \mu\text{m}^2$). The system without impurities is equivalent to the image shown in (C).

The indices i and j run over all particles. The radial distribution functions for the polyhedral, the impurity and the reference systems are shown in Fig. 3 A1) and B1). We observe for the polyhedrals that the peaks in the $g(r)$ are markedly broadened and that the structure in the $g(r)$ decays much faster with respect to the reference $g(r)$. Nevertheless, the clear differences between the $g(r)$ of the polyhedrals and the reference $g(r)$ are not due to polycrystallinity. The polyhedral particle-shape frustrates the hexagonal crystal on the single-particle level, leading to significant differences between the radial distribution functions [37]. Moreover, the differences in the radial distribution functions observed in Fig. 3 A1), are similar to those observed in single-crystalline regions [37]. Thus, the $g(r)$ is relatively insensitive to the presence of grain boundaries. This is corroborated by the impurity- $g(r)$, which appears to be rather similar to that of the reference system without impurities. Hence, in the impurity system the crystals are not frustrated on the particle level, leading to similar radial distribution functions for the impurity and reference system despite the presence of grain boundaries. Note that the difference between the reference radial distribution functions in Fig. 3 A1) and B1) is due to a difference in volume fraction. Recall that the polyhedral system has been analyzed after sedimentation had fully completed, in contrast to the impurity system. The volume fraction can be quantified in terms of the two-dimensional packing fractions ($\eta = N_T A_p / L^2$, with N_T the total number of particles in the image and L^2 the area of the image). Indeed, the more pronounced peaks in the reference $g(r)$ in Fig. 3 A1) (polyhedrals) correspond to a packing fraction of $\eta = 0.85$, which is clearly higher than $\eta = 0.74$ for the reference $g(r)$ in Fig. 3B1) (impurity system).

The loss of positional order shows up strongly in reciprocal space. The 2D structure factor is computed on a 2D grid of \mathbf{q} -values with a sampling rate of π/L with L the size of the microscopic image, as in [?]:

$$S_{\mathbf{q}} = \frac{1}{N} \left| \sum_{n=1}^N \exp(i(\mathbf{q} \cdot \mathbf{r}_n) \right| \quad (2)$$

with \mathbf{r}_n the particle coordinates and N the total number of particles. The structure factor profile $S(q)$ and the $g(r)$ profile are two related but distinctly different representations. As will be shown in more detail below, the $S(q)$ is more convenient for quantitative characterization of various types of long-range positional disorder, which is hidden in the details of the decay of the higher-order peaks of $g(r)$. The distinction between the finite-size effects (abrupt loss of the positional order) and the second-type disorder (monotonic deformation of the lattice) is extremely difficult on the basis of $g(r)$ but is easily obtainable from $S(q)$. The structure factors are presented in figure 4 A) and B) for, respectively, the polyhedrals and the reference spheres. Whereas the spheres are monocrystalline, the $S(q)$ for the polyhedrals is powderlike, with characteristic rings instead of sharp spots. A similar trend is observed for the impurity system and its reference system in figure 4D) and E). A notable difference between the impurity system and the polyhedral system shows up in the radially averaged profiles, shown for the polyhedral system and the impurity system and their reference systems in figure 4C) and figure 4F) respectively. As was clear from the $g(r)$ as well the positional order decays much faster in the polyhedral system. However, the angular profiles of the polyhedral system seem much wider than in the impurity system as well, which also follows from figure 4 A), where the intensity range used to depict the profile is much smaller than in figure 4B). This seems to point to orientational changes within the grain for the polyhedral system.

The bond-orientational correlation function $g_6(r)$ is significantly affected by the polycrystallinity, as is evident from Fig. 3A2) and B2). The bond-orientational correlation function $g_6(r)$ [47, 49] is defined as

$$g_6(r) = \langle \psi_6^*(0) \psi_6(r) \rangle \quad (3)$$

with

$$\psi_6(r_i) = \frac{1}{N} \sum_{j=1}^N \exp[6i\theta(r_{ij})]. \quad (4)$$

Here, ψ_6 is the local bond-orientational order parameter, where the summation j runs over all, in total N , near-

